Volume 17, Number 5, 2024. pp. 629-637

Jordan Journal of Physics

ARTICLE

Ionization Cross Section in Li^{2+} + H Collision

Saed J. Al Atawneh

Department of Physics, Zarqa University, Zarqa 13110, Jordan.

Doi: **https://doi.org/10.47011/17.5.10**

Received on: 20/06/2023; *Accepted on: 30/08/2023*

Abstract: We present total ionization cross section (TICS) and single differential ionization cross sections (SDCS) of neutral hydrogen atoms by partially stripped lithium ions. We employed a 4-body classical trajectory Monte Carlo (CTMC) model and a 4-body quasi-classical trajectory Monte Carlo (QCTMC) model. We present the TICS in the projectile impact energy range from 40 keV to 8 MeV, relevant to astronomical, plasma, and fusion research interests. We found that total ionization cross sections obtained using the CTMC model were lower than those calculated with QCTMC, and more closely aligned to previous experimental data. Furthermore, the QCTMC calculations show higher values than the experimental results but are closer to previous theoretical data. We also present the energy and angular differential ionization cross section of ground state hydrogen atom by Li^{2+} using both 4-body CTMC and 4-body QCTMC methods.

Keywords: Ion-atom collision, Ionization, Classical trajectory Monte Carlo method, Single differential ionization cross section.

1. Introduction

In the last 20 years, nuclear fusion research received great attention as a potential solution to humanity's energy challenges. In the nuclear fusion reactor, a huge number of impurities are present, such as carbon, lithium, and oxygen [1]. Recently, lithium has become increasingly recognized as a promising material for addressing divertor heat flux issues within fusion reactors. Ionized lithium atoms form highly radiative plasma layers, which can significantly decrease heat flow into divertor surfaces and thus decrease heatflux to them [1-6]. When evaporated lithium in its ionic form (partially stripped ions) interacts with different atoms such as hydrogen, carbon, deuterium, and oxygen, the probability of inelastic collisions involving multiply charged ions and neutral atoms increases. This has stimulated research into inelastic collisions, driven both by general scientific curiosity and their critical relevance to fusion applications [6–9]. For example, collisions between multiply charged ions and atomic hydrogen play a vital role in determining radiation losses, ionization rates, and beam penetration efficiency, all of which are essential for controlling heat flux to divertor surfaces in tokamak plasmas [5]. Consequently, accurate descriptions of the cross sections resulting from such collisions are crucial. In this study, we investigate collisions between neutral hydrogen targets and Li^{2+} ions (see Eq. 1):

$$Li^{2+} + H_T \rightarrow Li^{2+} + H_T^+ + e_T^- \quad (1)$$

The classical trajectory Monte Carlo (CTMC) method, developed in the early 1960s, marked a significant advancement in calculating cross

Corresponding Author: Saed J. Al Atawneh **Email**: salatawneh@zu.edu.jo

sections for atomic-molecular collisions with the advent of digital computers [10]. In this approach, atoms are modeled as classical particles moving within a quantum mechanical potential energy surface. The CTMC method is non-perturbative, relying on the numerical solution of classical equations of motion [11–16]. Later, Wilets *et al*. [17] introduced a classical model for nuclear collisions incorporating the Pauli Exclusion Principle through a momentum-dependent two-body potential. Building on this, Kirschbaum and Wilets [18] developed the quasi-classical trajectory Monte Carlo (QCTMC) model in 1980. This extension included a momentum-dependent potential, augmenting the pure Coulomb inter-particle potential to account for the Heisenberg uncertainty principle [24]. In the present work, both the classical trajectory Monte Carlo (CTMC) and quasi-classical trajectory Monte Carlo (QCTMC) models were employed [18–30]. We present total ionization cross sections (TICS) as well as energy and angular differential ionization cross sections. Additionally, single differential cross sections (SDCS) are provided to offer greater insight into the dynamics of the collisions [25].

To the best of our knowledge, no prior calculations for energy or angular differential ionization cross sections have been published for the ionization of hydrogen atoms by partially stripped lithium ion impact. Our calculations span a projectile energy range from 40 keV to 8 MeV, relevant to astrophysical, laboratory, and plasma research interests. Unless otherwise specified, atomic units are used throughout this work.

2. Theory

2.1. *The CTMC Models*

As is well-known, classical descriptions of collision processes work extremely well [26-31]. In this work, CTMC simulations were run using 4-body approximations [26-29]. Figure 1 depicts relative position vectors for 4-body collision systems. Li^{2+} in this case study is represented by two components: the ionic core of Li^{2+} and one active electron. All particles can be described by their masses and charges.

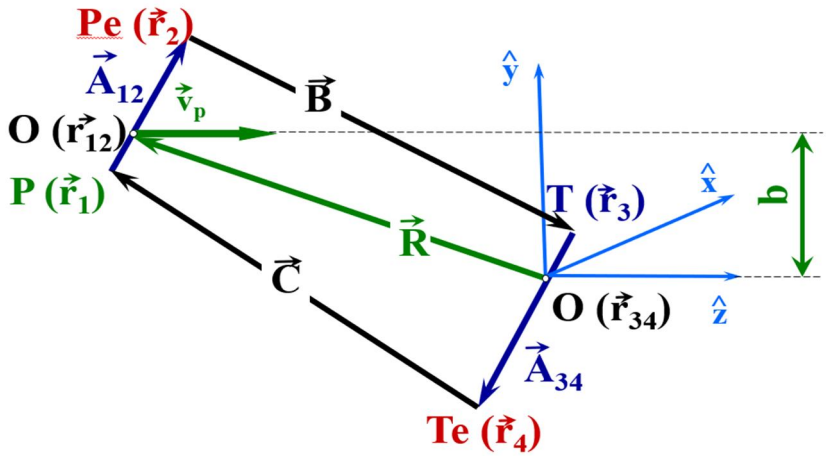

FIG. 1. The schematic diagram represents the relative position vectors for particles involved in our 4-body collision system. Here, $O(\vec{r}_{12})$ and $O(\vec{r}_{34})$ represent center-of-mass vectors for the target and projectile systems, respectively, while b denotes their impact parameter.

The initial electronic states can be determined by means of a microcanonical distribution. A microcanonical set represents the initial state of the target and projectile, compelled by their binding energy in any given shell, and can be described as follows:

$$\rho_{E_0}(\vec{A},\dot{\vec{A}}) = K_1\delta(E_0 - E) = \delta\left(E_0 - \frac{1}{2}\mu_{T,Te,P,Pe}\dot{\vec{A}}^2 - V(A)\right). \quad (2)$$

where K_1 is a normalization constant, E_0 is the ionization energy of the active electron, $V(A)$ represents the electron and ionic-core potential, A is the length of the vector $\vec{A}$, and μ_{T,T_eP,P_e} is the reduced mass of particles "T", "T_e", "P", and "P_e" [32]. According to Eq. (2), the electronic coordinates are restricted within intervals where Eq. (3) holds true.

$$\frac{1}{2}\mu_{Te}\dot{\vec{A}} = E_0 - V(A) > 0. \quad (3)$$

Hamilton equation is given by:

$$H_0 = T + V_{coul}, \quad (4)$$

where

$$T = \frac{\vec{P}_p^2}{2m_p} + \frac{\vec{P}_{pe}^2}{2m_{pe}} + \frac{\vec{P}_T^2}{2m_T} + \frac{\vec{P}_{Te}^2}{2m_{Te}}, \quad (5)$$

and

$$V_{coul} = \frac{Z_p Z_{Pe}}{|\vec{r}_p - \vec{r}_{Pe}|} + \frac{Z_P Z_T}{|\vec{r}_P - \vec{r}_T|} + \frac{Z_p Z_{Te}}{|\vec{r}_p - \vec{r}_{Te}|} + \frac{Z_{pe} Z_T}{|\vec{r}_{pe} - \vec{r}_T|} + \frac{Z_{Pe} Z_{Te}}{|\vec{r}_{pe} - \vec{r}_{Te}|} + \frac{Z_T Z_{Te}}{|\vec{r}_T - \vec{r}_{Te}|}, \quad (6)$$

where T and V_{coul}, respectively, stand for total kinetic energy and Coulomb potential term [27, 32]. $\vec{P}$, Z, $\vec{r}$, and m stand for the momentum vector, charge, position vector, and mass of each particle [27, 32]. Here are the equations of motion according to Hamiltonian mechanics:

$$\dot{\vec{P}}_p = -\frac{\delta H_0}{\delta \vec{r}_P} = \frac{Z_P Z_{Pe}}{|\vec{r}_p - \vec{r}_{Pe}|^3}(\vec{r}_P - \vec{r}_{Pe}) + \frac{Z_P Z_T}{|\vec{r}_P - \vec{r}_T|^3}(\vec{r}_P - \vec{r}_T) + \frac{Z_P Z_{Te}}{|\vec{r}_P - \vec{r}_{Te}|^3}(\vec{r}_P - \vec{r}_{Te}), \quad (7)$$

$$\dot{\vec{P}}_{Pe} = -\frac{\delta H_0}{\delta \vec{r}_{Pe}} = -\frac{Z_P Z_{Pe}}{|\vec{r}_P - \vec{r}_{Pe}|^3}(\vec{r}_P - \vec{r}_{Pe}) - \frac{Z_T Z_{Pe}}{|\vec{r}_T - \vec{r}_{Pe}|^3}(\vec{r}_T - \vec{r}_{Pe}) - \frac{Z_{Te} Z_{Pe}}{|\vec{r}_{Te} - \vec{r}_{Pe}|^3}(\vec{r}_{Te} - \vec{r}_{Pe}), \quad (8)$$

$$\dot{\vec{P}}_T = -\frac{\delta H_{H_0}}{\delta \vec{r}_T} = -\frac{Z_P Z_T}{|\vec{r}_P - \vec{r}_T|^3}(\vec{r}_P - \vec{r}_T) - \frac{Z_{Te} Z_T}{|Te - \vec{r}_T|^3}(\vec{r}_{Te} - \vec{r}_T) + \frac{Z_T Z_{Pe}}{|\vec{r}_T - \vec{r}_{Pe}|^3}(\vec{r}_T - \vec{r}_{Pe}), \quad (9)$$

$$\dot{\vec{P}}_{Te} = -\frac{\delta H_{H_0}}{\delta \vec{r}_{Te}} = -\frac{Z_P Z_{Te}}{|\vec{r}_P - \vec{r}_{Te}|^3}(\vec{r}_P - \vec{r}_{Te}) - \frac{Z_{Te} Z_T}{|Te - \vec{r}_T|^3}(\vec{r}_{Te} - \vec{r}_T) - \frac{Z_{Te} Z_{Pe}}{|\vec{r}_{Te} - \vec{r}_{Pe}|^3}(\vec{r}_{Te} - \vec{r}_{Pe}). \quad (10)$$

The Runge-Kutta method is typically utilized to numerically integrate equations of motion using an ensemble of approximately $5x10^6$ primary trajectories per energy [8, 26, 27, 32]. Such an ensemble typically is required in order to ensure statistical uncertainties of less than 5% [20-27]. The total and single differential ionization cross sections are given by:

$$\sigma = \frac{2\pi b_{max}}{N} \sum_j b_j, \quad (11)$$

and

$$\left(\frac{d\sigma}{d\Omega_e}\right) = \frac{b_{max}}{N\, \Delta\Omega_e} \sum_j b_j, \quad (12)$$

$$\left(\frac{d\sigma}{dE_e}\right) = \frac{b_{max}}{N\, \Delta E_e} \sum_j b_j. \quad (13)$$

Here, b_j is the impact parameter corresponding to the trajectory associated with an ionization process within energy interval ΔE and the emission angle interval $\Delta\Omega$ of the electron, and N is the total number of calculated trajectories. b_{max} is the maximum value for the impact parameter where the processes described can take place. However, in this study, the simulation was run for different impact energies using thousands of trajectories and we discovered that the optimal value of b_{max} is 15 au. The statistical uncertainty of the cross section can be calculated by:

$$\Delta\sigma = \sigma \left[\frac{N - N_P}{N\, N_P}\right]^{1/2}. \quad (14)$$

N_P is the number of trajectories that satisfy the criteria for the ionization process.

2.2. *The QCTMC Model*

The QCTMC model improves on the CTMC model by including a quantum correction term [8, 24, 32, 25]. In order to simulate the Heisenberg uncertainty and Pauli principle, two distinct potentials (V_H for Heisenberg and V_P for Pauli) are added to the standard Hamiltonian to represent a non-classical effect [8]. As a result, inter-particle interactions are enhanced. Thus:

$$H_{QCTMC} = H_0 + V_H + V_P, \quad (15)$$

where H_0 is the standard Hamiltonian [see Eq. (4)]. Correction terms for H_0 include:

$$V_H = \sum_{i=1}^{N} \frac{1}{m r_i^2} f\left(\vec{r}_i, \vec{p}_i; \xi_H; \alpha_H\right) \quad (16)$$

and

$$V_p = \sum_{i=1}^{N} \sum_{j=i+1}^{N} \frac{2}{m r_{ij}^2} f\left(\vec{r}_{ij}, \vec{p}_{ij}; \xi_p; \alpha_p\right) \delta_{s_i, s_j}, \quad (17)$$

where i and j index the electrons. Additionally, $r_{ij} = r_j - r_i$ and the relative momentum is determined as follows:

$$\vec{P}_{ij} = \frac{m_i \vec{p}_j - m_j \vec{p}_i}{m_i + m_j}. \quad (18)$$

Here, $\delta_{s_i, s_j} = 1$, if the i^{th} and j^{th} electrons have the same spin and 0 if they are different [8]. The particular form of potential is chosen as:

$$f\left(\vec{r}_{\lambda\nu}, \vec{p}_{\lambda\nu}; \xi, \alpha\right) = \frac{\xi^2}{4\alpha r_{\lambda\nu}^2 \mu_{\lambda\nu}} exp\left\{\alpha\left[1 - \left(\frac{\vec{r}_{\lambda\nu} \vec{p}_{\lambda\nu}}{\xi}\right)^4\right]\right\}. \quad (19)$$

Since hydrogen atoms consist of one electron and one proton, Heisenberg constraints were

implemented with specific scaling parameters, namely the hardness parameter ($\boldsymbol{\alpha_H}$ = 3.0) and the dimensionless constant ($\boldsymbol{\xi_H}$ = 0.9258), in the 4-body QCTMC model to apply the Heisenberg constraint with potential illustrated in Eq. (20):

$$f\left(\vec{r}_{T,Te},\vec{P}_{T,Te};\varepsilon_H,\alpha_H\right)= \frac{{\xi_H}^2}{4\alpha_H\vec{r}_{T,Te}^{\,2}\mu_{T,Te}} exp\left\{\alpha_H\left[1-\left(\frac{\vec{r}_{T,Te}\vec{P}_{T,Te}}{\xi_H}\right)^4\right]\right\}. \quad (20)$$

As with the target atom, the correction term must be considered for the projectile atom:

$$f\left(\vec{r}_{P,Pe},\vec{P}_{P,Pe};\varepsilon_H,\alpha_H\right)= \frac{{\xi_H}^2}{4\alpha_H\vec{r}_{P,Pe}^{\,2}\mu_{P,Pe}} exp\left\{\alpha_H\left[1-\left(\frac{\vec{r}_{P,Pe}\vec{P}_{P,Pe}}{\xi_H}\right)^4\right]\right\}. \quad (21)$$

As shown in Fig. 1, the equations of motion which incorporate Hamiltonian mechanics as well as the correction terms for cross section calculations can be expressed as:

$$\dot{\vec{P}}_p=-\frac{\delta H_{QCTMC}}{\delta\vec{r}_P}=\left[\frac{Z_PZ_{Pe}}{|\vec{r}_p-\vec{r}_{Pe}|^3}(\vec{r}_P-\vec{r}_{Pe})-\left(-\frac{{\xi_H}^2}{2\alpha_H\vec{r}_{P,Pe}^{\,4}\mu_{P,Pe}}-\frac{(\vec{P}_{P,Pe})^4}{\mu_{P,Pe}{\xi_H}^2}\right)exp\left\{\alpha_H\left[1-\left(\frac{r_{P,Pe}P_{P,Pe}}{\xi_H}\right)^4\right]\right\}\right]+\frac{Z_PZ_T}{|\vec{r}_P-\vec{r}_T|^3}(\vec{r}_P-\vec{r}_T)+\frac{Z_PZ_{Te}}{|\vec{r}_P-\vec{r}_{Te}|^3}(\vec{r}_P-\vec{r}_{Te}), \quad (22)$$

$$\dot{\vec{P}}_{Pe}=-\frac{\delta H_{QCTMC}}{\delta\vec{r}_{Pe}}=-\left[\frac{Z_PZ_{Pe}}{|\vec{r}_P-\vec{r}_{Pe}|^3}(\vec{r}_P-\vec{r}_{Pe})+\left(-\frac{{\xi_H}^2}{2\alpha_H\vec{r}_{P,Pe}^{\,4}\mu_{P,Pe}}-\frac{(\vec{P}_{P,Pe})^4}{\mu_{P,Pe}{\xi_H}^2}\right)exp\left\{\alpha_H\left[1-\left(\frac{r_{P,Pe}P_{P,Pe}}{\xi_H}\right)^4\right]\right\}\right]-\frac{Z_TZ_{Pe}}{|\vec{r}_T-\vec{r}_{Pe}|^3}(\vec{r}_T-\vec{r}_{Pe})-\left[\frac{Z_{Te}Z_{Pe}}{|\vec{r}_{Te}-\vec{r}_{Pe}|^3}(\vec{r}_{Te}-\vec{r}_{Pe})-\left(-\frac{{\xi_P}^2}{2\alpha_P\vec{r}_{Te,Pe}^{\,4}\mu_{Te,Pe}}-\frac{(\vec{P}_{Te,Pe})^4}{\mu_{Te,Pe}{\xi_H}^2}\right)exp\left\{\alpha_p\left[1-\left(\frac{r_{Te,Pe}P_{Te,Pe}}{\xi_P}\right)^4\right]\right\}\right], \quad (23)$$

$$\dot{\vec{P}}_T=-\frac{\delta H_{QCTMC}}{\delta\vec{r}_T}=-\frac{Z_PZ_T}{|\vec{r}_P-\vec{r}_T|^3}(\vec{r}_P-\vec{r}_T)-\left[\frac{Z_{Te}Z_T}{|Te-\vec{r}_T|^3}(\vec{r}_{Te}-\vec{r}_T)+\left(-\frac{{\xi_H}^2}{2\alpha_H\vec{r}_{T,Te}^{\,4}\mu_{T,Te}}-\frac{\vec{P}_{T,Te}^{\,4}}{\mu_{T,Te}{\xi_H}^2}\right)exp\left\{\alpha_H\left[1-\left(\frac{r_{T,Te}P_{T,Te}}{\xi_H}\right)^4\right]\right\}\right]+\frac{Z_TZ_{Pe}}{|\vec{r}_T-\vec{r}_{Pe}|^3}(\vec{r}_T-\vec{r}_{Pe}), \quad (24)$$

$$\dot{\vec{P}}_{Te}=-\frac{\delta H_{QCTMC}}{\delta\vec{r}_{Te}}=-\frac{Z_PZ_{Te}}{|\vec{r}_P-\vec{r}_{Te}|^3}(\vec{r}_P-\vec{r}_{Te})-\left[\frac{Z_{Te}Z_T}{|Te-\vec{r}_T|^3}(\vec{r}_{Te}-\vec{r}_T)+\left(-\frac{{\xi_H}^2}{2\alpha_H\vec{r}_{T,Te}^{\,4}\mu_{T,Te}}-\frac{\vec{P}_{T,Te}^{\,4}}{\mu_{T,Te}{\xi_H}^2}\right)exp\left\{\alpha_H\left[1-\left(\frac{r_{T,Te}P_{T,Te}}{\xi_H}\right)^4\right]\right\}\right]-\left[\frac{Z_{Te}Z_{Pe}}{|\vec{r}_{Te}-\vec{r}_{Pe}|^3}(\vec{r}_{Te}-\vec{r}_{Pe})-\left(-\frac{{\xi_P}^2}{2\alpha_P\vec{r}_{Te,Pe}^{\,4}\mu_{Te,Pe}}-\frac{(\vec{P}_{Te,Pe})^4}{\mu_{Te,Pe}{\xi_H}^2}\right)exp\left\{\alpha_p\left[1-\left(\frac{r_{Te,Pe}P_{Te,Pe}}{\xi_P}\right)^4\right]\right\}\right]. \quad (25)$$

3. Results and Discussion

3.1. Total Ionization Cross Section

In the present work, we focus on the ionization channels when the target charge decreases by one while the projectile is unchanged after the collision. Initially, a Li^{2+}+ H collision might cause the projectile or target to release one electron. The electron will be expelled into the continuum as shown by the equations below:

$$P+T\rightarrow\begin{cases}P+T^+ +e_T^-, & (26a)\\ P+T^+ +e_P^-, & (26b)\end{cases}$$

where P and T stand for the projectile and the target, respectively.

Classically, the ionization process can be divided into two distinct channels [14]. Direct ionization channel refers to one-step processes in which an interaction results in one particle losing an electron and its partner remaining unchanged after colliding; this channel can be described by Eq. (27):

$$(P,e_P^-)+(T,e_T^-)\rightarrow(P,e_P^-)+T^+ +e_T^-. \quad (27)$$

The second classical channel, which yields the same final particles, involves two-step multi-electron interactions [32]. One electron from a target can be captured and transferred onto the projectile's bound state while one projectile electron becomes free during collision [32], as illustrated by Eq. (28):

$$(P,e_P^-)+(T,e_T^-)\rightarrow(P,e_T^-)+T^+ +e_P^-. \quad (28)$$

Figure 2 depicts our current total ionization cross sections, a summation of the single- and two-step ionization cross sections, for hydrogen targets exposed to partially stripped lithium (Li^{2+}) ions as a function of impact energy, along with previous results by Purkait [33], Shah and Gilbody [34], and McGuir [35]. McGuire [35]

calculated the ionization cross sections of the H-target by Li^{2+} and Li^{3+} ions using a plane wave approximation that includes provisions for electron screening of incident ions. Later, Purkait [33] calculated the charge transfer and ionization cross sections of ground-state hydrogen atoms by ions of lithium, Li^{q+} $(q \leq 3)$ at energies between 30-200 keV/amu using classical (CTMC method) and quantum mechanical (BCCIS approximation) approaches, making a notable advancement over previous theories by incorporating non-Coulombic model potentials to account for interactions between the active electron and the partially stripped projectile ion.

The present CTMC results for the total ionization cross section (TICS) show good agreement with the TICS obtained using the CTMC/quantum methods by Purkait [33] at low-impact energies. Furthermore, our CTMC results align excellently with experimental TICS data obtained by Shah and Gilbody [34], particularly within the energy range of 0.37 MeV to 24 MeV.

Furthermore, both CTMC and QCTMC models agreed well with previous experimental and theoretical data with regard to single-step (direct ionization) processes. Contrastingly, two-step processes exhibited lower probabilities for CTMC and QCTMC approaches than other results. For the CTMC method, this can be justified by the tendency of a classical atom to collapse or autoionize due to the absence of threshold energy imposed by quantum mechanics. For the QCTMC method, the underestimation of two-step processes is possibly due to the repulsive nature of the Heisenberg potential. This potential restricts particles from entering quantum mechanically forbidden regions of phase-space $(\vec{r}, \vec{p})$, thereby reducing the probability of these interactions.

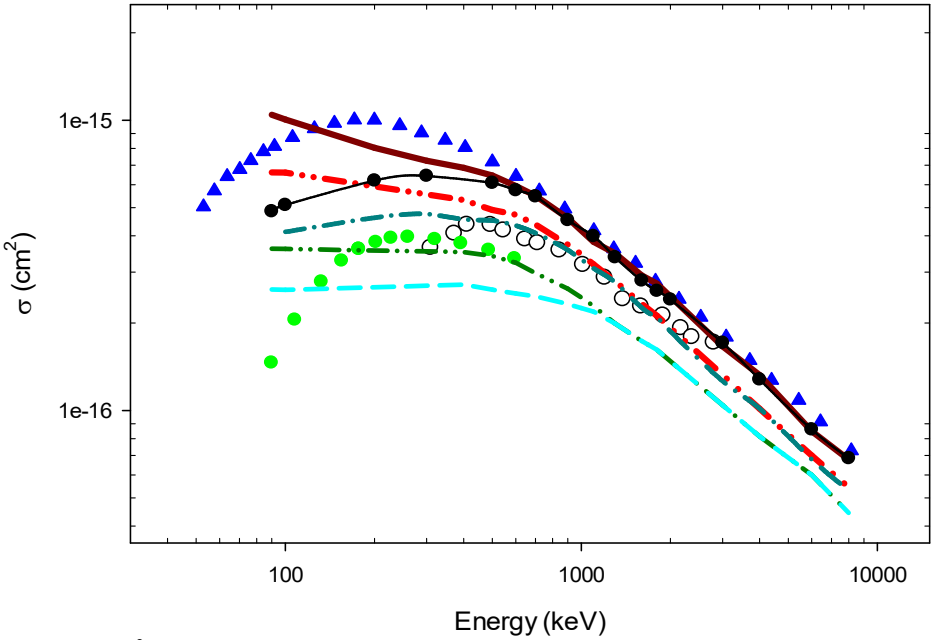

FIG. 2. The TICS of Li^{+2} + H collision as a function of impact energy. Red dashed-dot-dot: the total ionization cross sections results (CTMC). Dark cyan dashed-dots: single-step process results (CTMC). Cyan dashed line: two-step process results (CTMC). Dark red solid line: the total ionization cross sections results (QCTMC). Black circles-solid line: single-step process results (QCTMC). Dark green dash-dot-dot: two-step process results (QCTMC). Blue triangles: plane-wave Born approximations by McGuir [35]. Green dots: Classical/Quantum approximation data by Purkait [33]. Open circles: experimental data by Shah and Gilbody [34].

3.2. Single Differential Ionization Cross Section

For ionization calculations, the impact parameters up to 15 au have been found necessary for accurate calculations, in order to achieve convergence in terms of both energy and angular differential cross sections, with an agreement rate of over 98% between integrated SDCSs and total cross sections relating to ionization.

Figure 3 shows results for SDCS of hydrogen atoms as a function of electron-ejected energy by partially stripped lithium ions (Li^{2+}) using CTMC and QCTMC models at 600 keV impact energy. Figure 3 also shows that the peak

probability for electron ejection occurs around 3 au, where the probabilities of ejected electrons are decreased logarithmically with electron-ejected energy. The results are shown in the center of mass frame. The QCTMC results show a higher cross section in comparison to standard CTMC calculations, demonstrating the role of Heisenberg correction. On the other hand, the two-step process has a lower probability due to the classical atom's tendency to autoionize, as observed in the total ionization cross sections calculation.

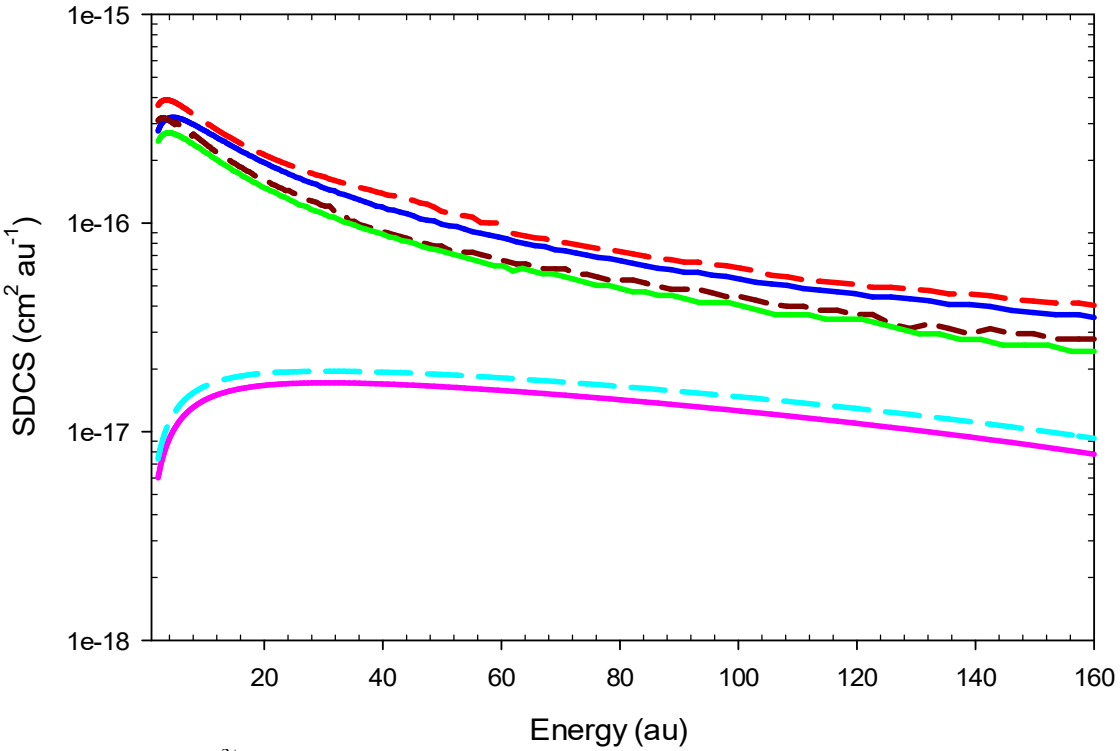

FIG. 3. The SDCS of Li^{2+}+ H collision as a function of electron-ejected energy at 600 keV impact energy. Red dashed line: presents QCTMC results, a summation of single and two-step processes. Blue solid line: presents CTMC results, a summation of single and two-step processes. Dark red dashed line: single-step process results (QCTMC). Green solid line: single-step process results (CTMC). Cyan dashed line: two-step process results (QCTMC). Pink solid line: two-step process results (CTMC).

Figure 4 shows results for SDCS of hydrogen atoms as a function of the electron-ejected energy by partially stripped lithium ions (Li^{2+}) using CTMC and QCTMC models at 900 keV impact energy. Figure 4 also shows the probability peak of electron-ejected energy around 1.34 au. As noticed, the probability peak of electron-ejected energy at 900 keV impact energy is lower than that of 600 keV impact energy because the incident charged particles (projectiles) transferred momentum to bound electrons proportional to the product of the Coulombic force and the time spent by the projectile in the proximity of the atom. High-energy ions transfer less momentum due to the shorter time spent in the vicinity of the orbital electron. The results, plotted in the center-of-mass frame, align with expectations. The QCTMC results demonstrate higher cross sections compared to standard CTMC calculations, highlighting the enhancement provided by the Heisenberg correction term. Regardless of the projectile impact energy, the two-step process cross sections exhibit similar trends, reinforcing the consistency of these findings across different energy levels.

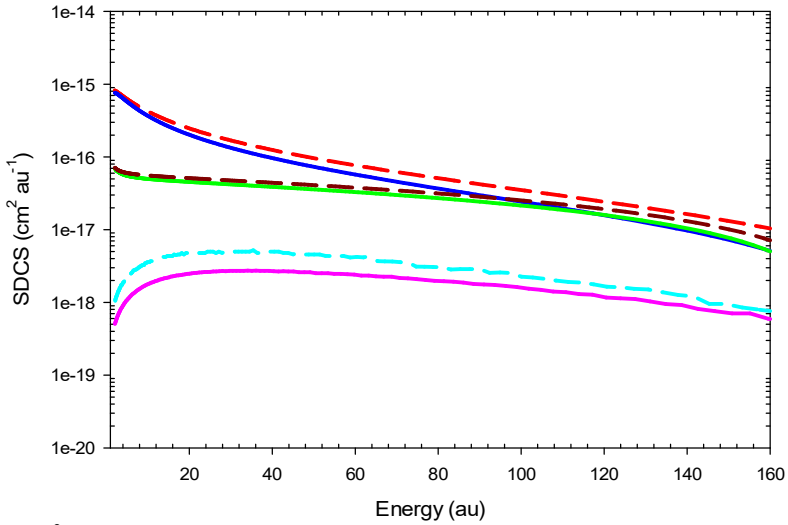

FIG. 4. The SDCS of Li^{2+}+ H collision as a function of electron-ejected energy at 900 keV. Red dashed line: QCTMC results, a summation of single and two-step processes. Blue solid line: CTMC results, a summation of single and two-step processes. Dark red dashed line: single-step process results (QCTMC). Green solid line: single-step process results (CTMC). Cyan dashed line: two-step process results (QCTMC). Pink solid line: two-step process results (CTMC).

Figures 5 and 6 depict SDCS for neutral hydrogen atoms as a function of electron ejected angle using CTMC and QCTMC models at selected impact energies. Figures 5 and 6 also show the probability peak of the electron ejected angle at around 0 degrees (forward direction). As noticed, at low-impact energy, the probability of electron ejection in the forward direction is large because the time of collision is so long (slow collision), see Fig. 5. In contrast, at high-impact energy, the probability peak of electron ejection angle is small (see Fig. 6) due to the fact that the momentum transfer to the bound electrons is relatively small, as the incident projectile spends less time near target atom (fast collision, $v_P \gg v_{eT}$). Generally, the SDCS as a function of electron ejected angle decrease logarithmically with angles to reach the minimum value at 130 degrees. On the other hand, the back-ejected ionization probability (head-on collision) appears at 180 degrees and this process strongly occurs at small impact parameters. The QCTMC calculations, as expected, show larger cross sections than the standard CTMC model, confirming the importance of the Heisenberg correction term. However, no previous theoretical or experimental data were available for comparison.

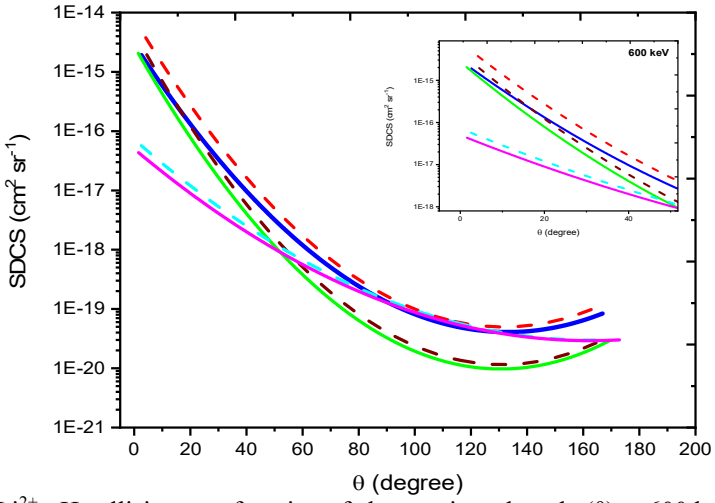

FIG. 5. The SDCS of Li^{2+}+ H collision as a function of electro-ejected angle (θ) at 600 keV impact energy. Red dashed line: QCTMC results, a summation of single and two-step processes. Blue solid line: CTMC results, a summation of single and two-step processes. Dark red dashed line: single-step process results (QCTMC). Green solid line: single-step process results (CTMC). Cyan dashed line: two-step process results (QCTMC). Pink solid line: two-step process results (CTMC).

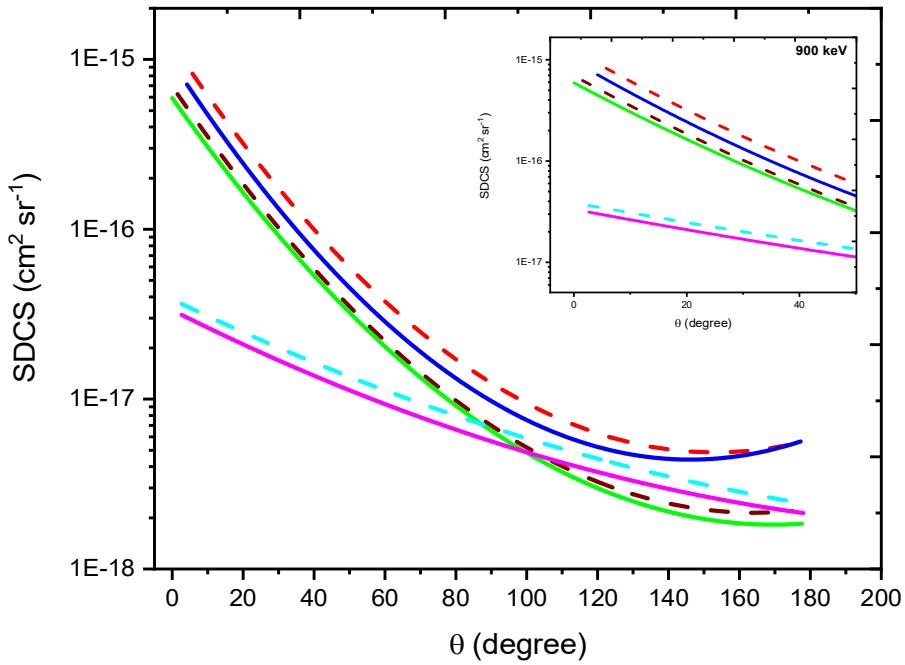

FIG. 6. The SDCS of Li^{2+}+ H collision as a function of electron-ejected angle (θ) of 900 keV impact energy. Red dashed line: QCTMC results, a summation of single and two-step processes. Blue solid line: CTMC results, a summation of single and two-step processes. Dark red dashed line: single-step process results (QCTMC). Green solid line: single-step process results (CTMC). Cyan dashed line: two-step process results (QCTMC). Pink solid line: two-step process results (CTMC).

4. Conclusion

We presented the total ionization as well as energy and angular differential ionization cross sections in Li^{2+}+ H collision using both 4-body CTMC and 4-body QCTMC approaches. Our calculations focused on energy ranging from 40 keV to 8 MeV where cross sections could potentially be of relevance for fusion research and astronomical physics. We found a good agreement between the TICS of CTMC and QCTMC calculations with the available experimental and theoretical data. The QCTMC calculations showed a good agreement with both classical/quantum approximation data in the 200–500 keV range, as well as with plane-wave Born approximation (PWB) results. Finally, we presented the SDCS of Li^{2+}+ H collision for selected energies using both 4-body CTMC and 4-body QCTMC models. We found that the probability peak of electron-ejected energy is 3 au and 1.34 au for 600 keV and 900 keV impact energies, respectively. Last, but not least, we showed that the probability peak of the electron-ejected angle is inversely proportional to the impact energy of the incident projectile.

Acknowledgment

This work was conducted without external funding.

References

[1] Ono, M., “Lithium As Plasma Facing Component for Magnetic Fusion Research”. (Nova Scientific Publications, August 2012); (Princeton Plasma Physics Lab. (PPPL), Princeton, NJ (United States). p. Medium: ED).

[2] Skokov, V.G., Sergeev, V.Y., Anufriev, E.A., and Kuteev, B.V., Tech. Phys., 66 (2021) 664.

[3] Goldston, R.J., Myers, R., and Schwartz, J., Phys. Scr., T167 (2016) 014017.

[4] Kaita, R., Plasma Phys. Control. Fusion. 61 (2019) 113001.

[5] Rognlien, T.D. and Rensink, M.E., Phys. Plasmas, 9 (2002) 2120.

[6] Mirnov, S.V., Azizov, E.A., Evtikhin, V.A., Lazarev, V.B., Lyublinski, I.E., Vertkov, A.V., and Yu Prokhorov, D., Plasma Phys. Control. Fusion., 48 (2006) 821.

[7] Shipsey, E.J., Browne, J.C., and Olson, R.E., J. Phys. B: At. Mol. Opt. Phys., 14 (1981) 869.

[8] Atawneh, S.J.A. and Tőkési, K., Nucl. Fusion., 62 (2021) 026009.

[9] McCullough, R.W., Gillen, D.R., Voulot, D., Kearns, D.M., and Gilbody, H.B., Phys. Scr., T92 (2001) 76.

[10] Blais, N.C. and Bunker, D.L., J. Chem. Phys. 37 (1962) 2713.

[11] Abrines, R. and Percival, I.C., Proc. Phys. Soc. London, 88 (1966) 861.

[12] Atawneh, S.J.A. and Tőkési, K., Atomic Data and Nuclear Data Tables, 146 (2022)101513.

[13] Olson, R.E. and Salop, A., Phys. Rev. A, 16 (1977) 531.

[14] Atawneh, S.J.A., Eur. Phys. J. Plus, 139 (2024) 902.

[15] Tőkési, K. and Hock, G., J. Phys. B, 29 (1996) L119.

[16] Atawneh, S.J.A., Atoms, 12 (2024) 63.

[17] Wilets, L., Henley, E.M., Kraft, M., and Mackellar, A.D., Nucl. Phys. A, 282 (1977) 341.

[18] Atawneh, S.J.A., Asztalos, Ö., Szondy, B., Pokol, G.I., and Tőkési, K., Atoms, 8 (2020) 31.

[19] Atawneh, S.J.A. and Tőkési, K., J. Phys. B: At. Mol. Opt. Phys., 54 (2021) 065202.

[20] Kirschbaum, C.L. and Wilets, L., Phys. Rev. A, 21 (1980) 834.

[21] Wilets, L. and Cohen, J.S., Contemp. Phys., 39 (1998) 163.

[22] Velayati, A. and Ghanbari-Adivi, E., Eur. Phys. J. D, 72 (2018) 100.

[23] Velayati, A., Ghanbari-Adivi, E., and Ghorbani O., J. Phys. B: At. Mol. Opt., 51 (2018) 185201.

[24] Atawneh, S.J.A., PhD dissertation. ProQuest, http://hdl.handle.net/2437/329082.

[25] Mori, N.A., Utamuratov, R., Fursa, D.V., Zammit, M.C., and Bray, I., J. Phys. B: At. Mol. Opt., 54 (2021) 015205.

[26] Olson, R.E., Reinhold, C.O., and Schultz, D.R., Proceedings of the 4th Workshop on High-Energy Ion-Atom Collision Processes, Debrecen, Hungary, 17-19 September 1990, Eds. D. Berenyi and G. Hock, Lecture Notes in Physics (1991), Vol. 376, p. 69.

[27] Oliveira, V., Herbert, A., Santos, A.C.F., and Tőkési, K., Eur. J. Phys. D, 73(2019) 146.

[28] Abrines, R. and Percival, I.C., Proc. Phys. Soc., 88 (1966) 861.

[29] Tökési, K., Paripás, B. and Kovács, E., Eur. J. Phys. D, 73 (2019) 84.

[30] Tokési, K. and Hock, G., Nucl. Instrum. Methods Phys. Res. Sect. B, 86 (1994) 201.

[31] Janev, R.K. and McDowell, M.R.C., Phys. Lett. A, 102 (1984) 405.

[32] Atawneh, S.J.A. and Tőkési, K., Phys. Chem. Chem. Phys., 24 (2022) 15280.

[33] Purkait, M., Nucl. Instr. Methods Phys. Res. B, 207 (2003) 101.

[34] Gillespie, G.H., Phys. Lett. A, 72 (1979) 329.

[34] Shah, M.B. and Gilbody, H.B., J. Phys. B: At. Mol. Opt. Phys., 15 (1982) 413.

[35] McGuire, J.H., Private communication (1981).